

Melting and orientational epitaxy in argon and xenon monolayers on graphite

K. L. D'Amico

*Department of Physics, Brookhaven National Laboratory, Upton, New York, 11973-5000
and Corporate Research Laboratories, Exxon Research and Engineering Company,
Clinton Township, Route 22 East, Annandale, New Jersey 08801*

J. Bohr

*Department of Physics, Risø National Laboratory, DK-4000 Roskilde, Denmark
and Department of Physics, Brookhaven National Laboratory, Upton, New York 11973-5000*

D. E. Moncton

*Corporate Research Laboratories, Exxon Research and Engineering Company,
Clinton Township, Route 22 East, Annandale, New Jersey 08801*

Doon Gibbs

*Department of Physics, Brookhaven National Laboratory, Upton, New York 11973-5000
(Received 14 April 1989; revised manuscript received 9 November 1989)*

We have studied the melting behavior for Ar at a coverage of $\rho \sim 0.81$ and the orientational-epitaxy effect for Ar and Xe. We find that the Ar melts continuously from a rotated incommensurate solid to a rotated fluid phase; the fluid with positional correlations of 400 \AA is rotated by $\sim 2^\circ$. The melting behavior agrees well with that observed by x-ray diffraction using a ZYX-graphite substrate, and is consistent with the heat-capacity data of Migone *et al.* For Xe, the orientational-epitaxy data show a rotation to zero for increasing misfit magnitude, contrary to the Ar and Kr behavior. This is discussed in light of the role of entropy in the structure of this system.

INTRODUCTION

The rare gases adsorbed on the (001) surface of graphite offer perhaps the simplest and best studied monolayer systems known. In particular, they have been studied in an effort to understand one of the most basic of phase transitions: melting. While a great deal of effort has been devoted to this problem of the melting of a two-dimensional (2D) solid adsorbed on a substrate,¹⁻⁴ a concise, universal picture has not yet emerged. Indeed it is apparent from the vast body of experimental data that the salient differences between the properties of the most studied rare gases on graphite Ar, Kr, and Xe lead to qualitatively different behavior. For example, these rare gases differ in their relative strength of interaction with the graphite substrate.^{5,6} Further, the period of the overlayer competes with the period of the graphite substrate. These interactions lead to commensurate, incommensurate, and orientational-epitaxy phases. The very existence of these phases implies that the interplay between the substrate and the adsorbate is fundamental to the physics of these systems and cannot be ignored in discussion of their phase transitions. In this paper we discuss experiments performed on the melting transition of monolayer Ar on single-crystal graphite and on the orientational-epitaxy phases of both Ar and Xe monolayers.

Monolayers of Ar have been studied by numerous experimental techniques, including neutron⁷ and x-ray^{8,9} diffraction, LEED¹⁰ (low-energy electron diffraction), and

heat-capacity measurements.^{11,12} The heat-capacity study by Migone *et al.* shows peaks which provide evidence for successive transitions in the Ar monolayer.¹² The first is a small and sharp peak which is superimposed upon a dominating broad peak. They identify the first sharp (0.3 K FWHM) peak as being due to a first-order melting transition for the solid, and the broad peak as perhaps being associated with a more continuous loss of residual order in the system. This interpretation contrasts with other data on the system. Extensive x-ray data indicate a continuous melting transition.^{8,9} The line shape in the diffraction experiment evolves continuously from that of a finite-size limited solid peak to that of a peak for a fluid with a $\sim 50 \text{ \AA}$ correlation length.

One question that neither of these studies could address concerned orientational epitaxy in this system. LEED data for Ar adsorbed on single-crystal graphite clearly indicated that the solid overlayer had its symmetry axis rotated with respect to the graphite substrate;¹⁰ the angle was observed to be $\sim 3^\circ$. These data provided the first experimental evidence for a rotated phase in a rare-gas-graphite system, and confirmed the theoretical prediction of Novaco and McTague.^{13,14} In addition, the LEED data suggested that the finite rotation angle was maintained into the fluid phase.¹⁵ Clearly, a measurement which could simultaneously address the melting and orientational-epitaxy behavior was required. In this work we have performed an experiment on Ar adsorbed on single-crystal graphite, where we have used synchrotron x-ray diffraction to study both phenomena.

In addition, we present orientational-epitaxy data for Xe. The melting behavior has been extensively investigated and a continuous transition is inferred for coverages significantly larger than a monolayer. First order melting is observed in the submonolayer regime.^{8,16,17,18}

Single-crystal x-ray diffraction data show that the continuous melting of Xe takes place from an aligned solid phase¹⁸ (orientational-epitaxy angle is equal to zero), yet Xe has been shown to possess a rotated solid phase.¹⁹ Thus, there exists a qualitative difference between the Ar and Xe systems. The main results of our study are as follows: A continuous melting transition is observed for Ar; the melting occurs from a rotated phase, through a rotated fluid with correlation lengths larger than ~ 400 Å. In contrast to Ar, Xe possesses an orientationally epitaxied phase at low temperature, and the rotation angle goes to zero with increasing temperature prior to the melting temperature.

EXPERIMENTAL APPROACH

The experiments were performed at Beamline VII-2 at the Stanford Synchrotron Radiation Laboratory (Palo Alto, CA); beamline hardware were as previously described.²⁰ The details of the cryostat and gas-handling system used for this single-crystal graphite adsorption study have been described in detail and were the same as has been used in previous studies,^{19,21} with one additional feature. For this study we have added ~ 0.1 g of graphite foam (Vermicular graphite) to the cell. The three-dimensional (3D) vapor pressure of the Ar in equilibrium with the monolayer is so low that it is impossible to control externally by, e.g., a leak valve. The graphite foam provides a buffer whose surface area can be determined by a standard isotherm; the foam can then be filled with a known coverage thus providing a well-defined 3D vapor in equilibrium with the single crystal. The vermicular graphite foam used was baked in a vacuum of $\sim 10^{-6}$ Torr at $\sim 700^\circ\text{C}$ for six hours prior to loading into the cell under a dry N_2 atmosphere. The entire gas handling system, including graphite foam, was then baked to $\sim 120^\circ\text{C}$ prior to the experiment on the single crystal. Both Ar and Kr isotherms were measured and the effective surface area was determined by calibration against previous Ar and Kr isotherm and diffraction data.²²

About 1 Torr pressure of He gas was added to the cell after the Ar fill. This was done to provide an efficient path for thermal conduction between the single-crystal and the graphite foam, assuring that the two were in thermal equilibrium. Finally, the graphite single crystal was flashed to $\sim 600^\circ\text{C}$ to clean it *in situ* by passing a current through it.

A typical Ar isotherm is shown in Fig. 1. The fill is in arbitrary units, but the fill required for one commensurate Kr monolayer (a coverage of $\rho=1$) is equal to 12.4 in these units. A dead volume correction has been applied to the Ar fill, the dead volume in the cell as a function of temperature having been determined with a He isotherm measurement.

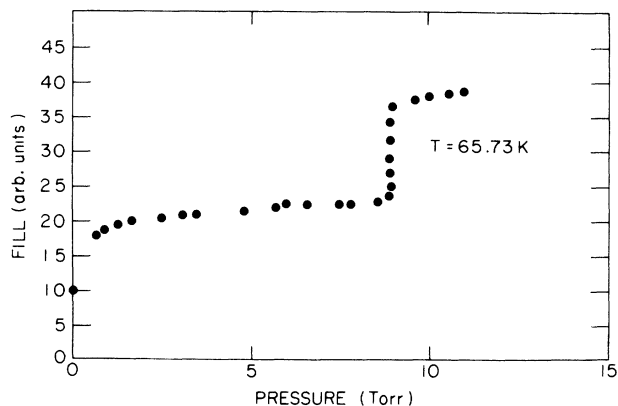


FIG. 1. A typical isotherm for Ar on the graphite-foam substrate measured at a temperature of 65.73 K. A dead-volume correction for the cell, determined by measuring a He isotherm at 66 K, has been applied to the data.

RESOLUTION STUDIES USING COMMENSURATE Kr

To characterize the mosaic and finite-size qualities of the single crystal, scans of commensurate solid Kr were performed at a coverage ρ of less than 1 (see Figs. 2 and 3). Since a commensurate 2D solid has true long-range positional order, the diffraction peak from the Kr provides both the radial (Fig. 2) and angular (Fig. 3) resolution function of the combined system consisting of a spectrometer plus graphite sample. The Kr radial scan width is close to that of the instrument;²⁰ this implies a finite crystallite size for the single crystal of $\sim 10\,000$ Å. Similarly, the angular scan of Fig. 3, performed by rocking the incident angle at fixed scattering angle such that $q=1.703$ Å⁻¹, is a measure of the mosaic distribution of the crystallites which comprise the *surface* of the graph-

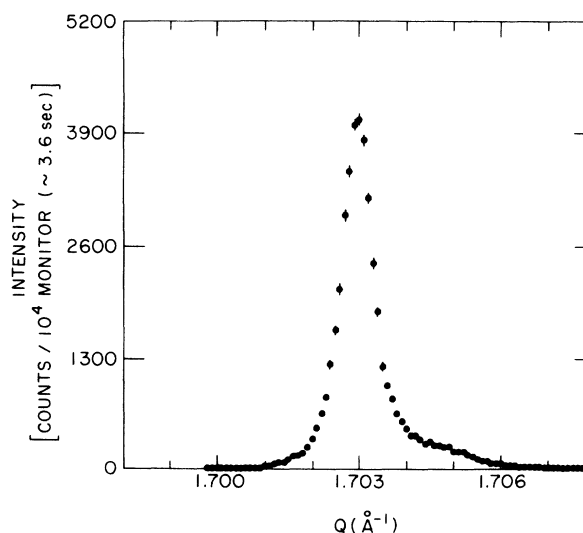


FIG. 2. Radial ($2\theta-\theta$) scan for commensurate Kr adsorbed on the single-crystal substrate at $T=89$ K and $p=0.6$ Torr; the peak full width at half maximum is 0.0008 Å⁻¹. The tail on the high- q side of the peak is due to the mosaic of the graphite crystal.

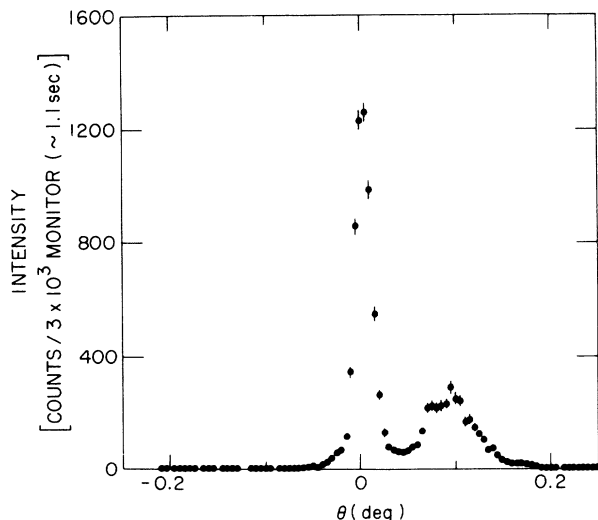


FIG. 3. Angular (θ) scan for commensurate Kr as in Fig. 2. The mosaic consists of two peaks, separated by 0.09° , with widths of 0.025° and 0.06° FWHM.

ite sample. One can see that the mosaic consists of two main peaks, separated by $\sim 0.09^\circ$, with widths of $\sim 0.025^\circ$ and 0.06° FWHM. In addition, this angle scan provides a means of aligning the crystal: the commensurate Kr (10) diffraction peaks occur along the graphite [110]. The rotated peaks of the orientationally epitaxially incommensurate solid occur at finite rotation angles with respect to this direction.

The commensurate Kr radial and angular scans were used as the resolution function for the system. Subsequent Ar and Xe radial and angle scans $S(x)$ were least-squares fitted to model line shapes by convoluting the model function $M(x)$ with the measured resolution function $R(x)$ from the scans in Figs. 2 and 3:

$$S(x) = \int_{-\infty}^{\infty} R(x')M(x-x')dx', \quad (1)$$

where x is either momentum transfer q or angle θ .

Ar MELTING AND ROTATION

For the Ar melting and rotation study, the foam was filled to a coverage of $\rho=0.81$. This resulted in an adsorbed layer which melted at ~ 50 K. Under these conditions the Ar solid is always in the rotated phase; we measured a rotation angle θ in the range $2.0^\circ < \theta < 3.0^\circ$. Here, the rotation angle θ is relative to the substrate [110], or the commensurate Kr [10]. Thus the Ar (10) peak is in fact a doublet of peaks rotated by $\pm\theta$ with respect to the graphite [110]. A radial scan through one of these peaks at $T=44.28$ K is shown in Fig. 4, and angle scan in Fig. 5. By comparison with the Kr scans in Figs. 2 and 3, one can see that the scans are nearly as sharp as the Kr scans in both radial and angular directions. Efforts to fit both scans in the solid phase to power law, Lorentzian, and Gaussian line shapes were made. Strictly speaking, the power law line shape $M(q)=q^{\eta-2}$ is the correct description for a 2D solid, however efforts to fit this line shape in the solid phase were frustrated by a lack of sufficient

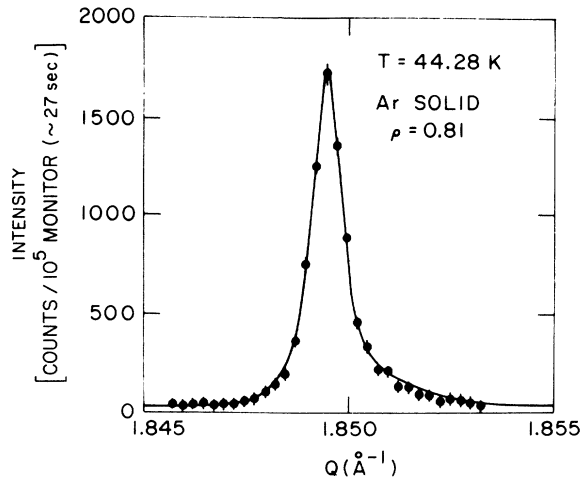


FIG. 4. Radial scan for solid Ar at $T=44.28$ K and coverage $\rho=0.81$. The solid line is a fit to a Lorentzian line shape convoluted with the experimental resolution function as discussed in the text.

counting statistics in the wings of the peak, where the power-law line shape manifests itself most prominently.

Therefore the Lorentzian line shape was used and this fit the data satisfactorily. As has been seen in previous studies using graphite as a substrate, the Lorentzian provides a good way to parametrize the solid line shape despite the fact that it is not believed to be the strictly correct functional form.¹⁶

Figures 6 and 7 show q and θ scans for a series of temperatures through the melting transition. The gradual broadening of the line shape is apparent in both directions. The signal became immeasurably small above 50.03 K. At that point the peak intensity had decreased to $< 1/50$ of the maximum intensity in the solid phase. Plots of the radial HWHM, κ_{radial} , and the excess angular width, $\kappa_{\text{excess}} = \kappa_{\text{transverse}} - \kappa_{\text{radial}}$, are shown versus temper-

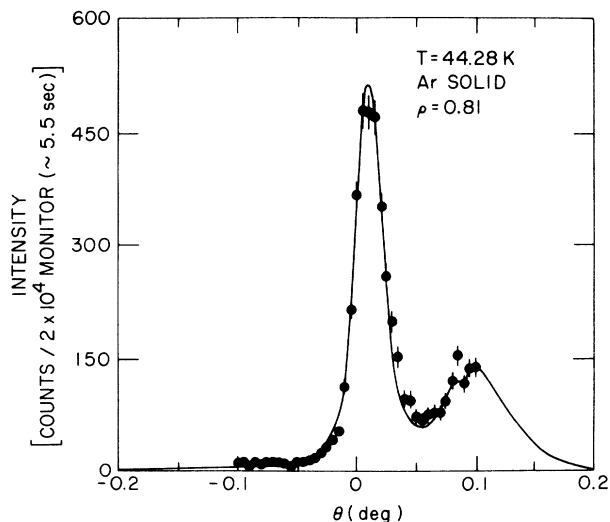


FIG. 5. Angular scan through the peak in Fig. 4; the solid line is a fit to a Lorentzian line shape convoluted with the measured graphite mosaic.

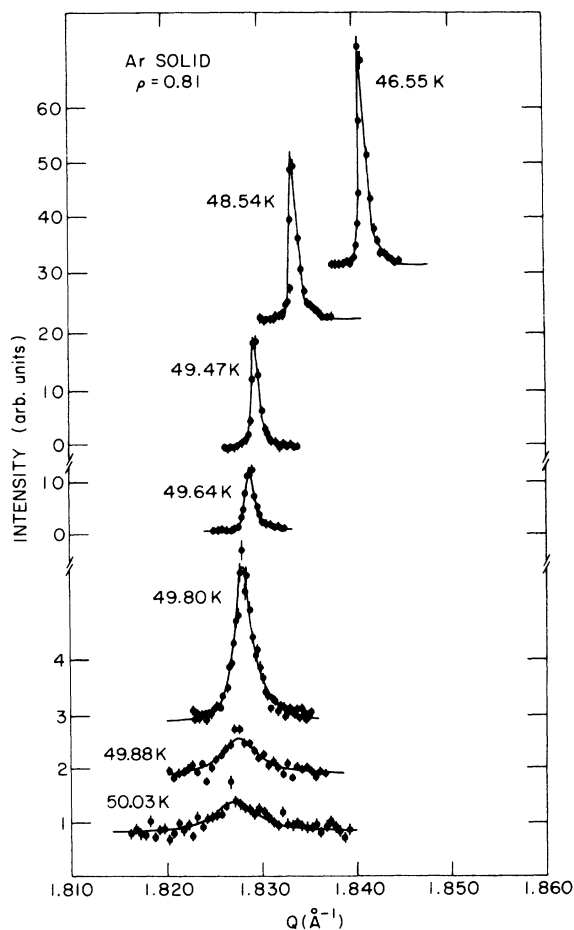


FIG. 6. Series of radial scans for Ar at coverage $\rho=0.81$ as a function of temperature; solid lines represent Lorentzian line-shape fits, with temperatures as noted. Lower three scans have a scale change of a factor of 10.

ature in Figs. 8 and 9. Here κ_{radial} is the fitted Lorentzian HWHM of the radial peak, and $\kappa_{\text{transverse}}$ is equal to the momentum transfer multiplied by the fitted angular HWHM. The peaks evolved from the width in the solid to a fluid phase with a positional correlation length $1/\kappa_{\text{radial}}$ of ~ 400 Å over a range of ~ 0.3 K.

Accompanying the melting transition is a change in the orientational epitaxy angle. Figure 10 shows a plot of orientational angle versus T , with the fluid phase points indicated. We thus have the unique result that the solid melts from a rotated orientation to a rotated fluid; when the fluid correlation length is 400 Å, the fluid has a rotation angle of $\sim 2.0^\circ$. It should be noted that additional angle scans were performed around the symmetry direction, $\theta_{\text{rot}}=0^\circ$. No evidence of an unrotated fluid or solid phase was seen.

A plot of rotation angle versus percent misfit for Ar, Kr, and Xe (see below) is shown in Fig. 11. The Kr data are from Ref. 21. The percent misfit m is defined with respect to the commensurate lattice constant d_0 or commensurate wave vector q_0 , as

$$m = 100 \frac{d_0 - d}{d_0} \quad \text{or} \quad m = 100 \frac{q - q_0}{q}, \quad (2)$$

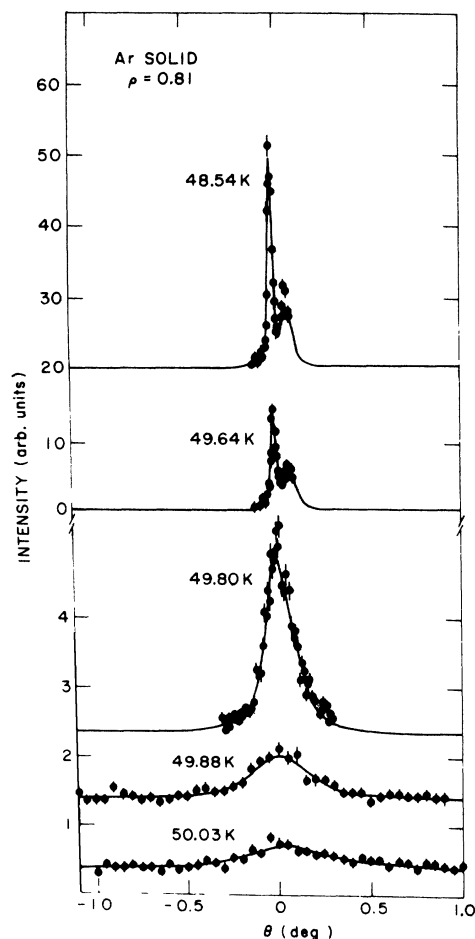


FIG. 7. Series of angular scans for Ar at coverage $\rho=0.81$ with temperatures as noted. Solid lines are Lorentzian line-shape fits. Lower three panels have a scale change of a factor of 10.

κ_{RADIAL} vs TEMPERATURE
Ar MELTING $\rho=0.81$

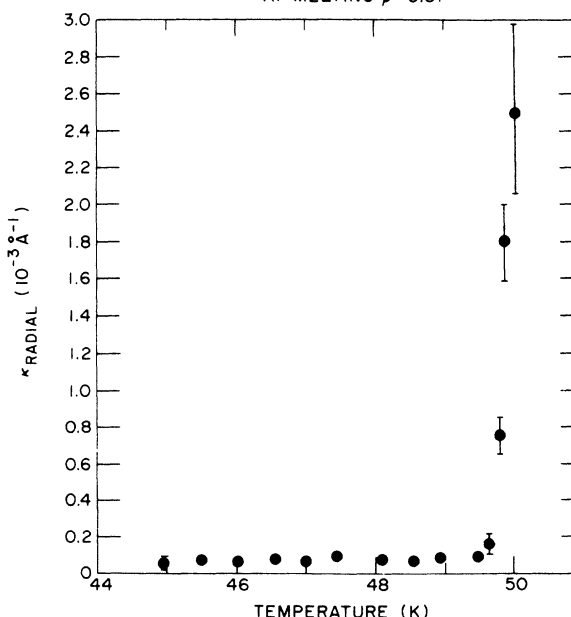


FIG. 8. Plot of the fitted radial Lorentzian HWHM κ_{radial} vs temperature for Ar melting at coverage $\rho=0.81$.

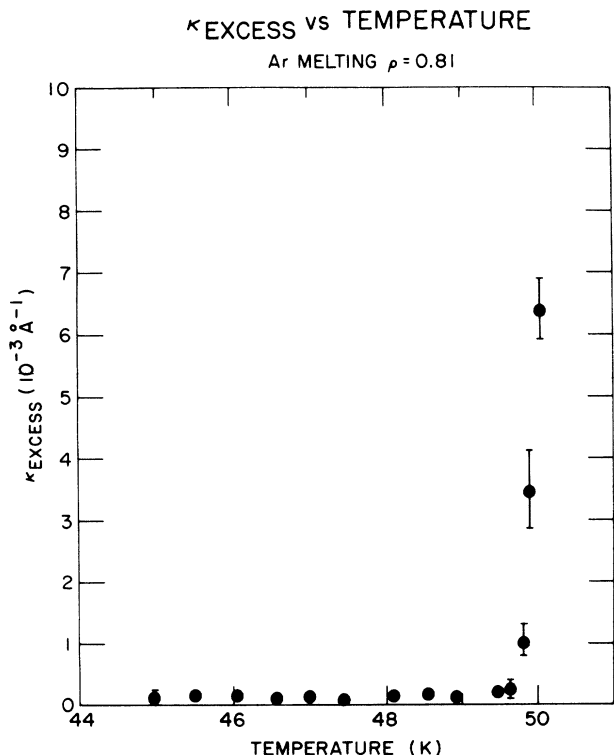


FIG. 9. Plot of the excess angular width κ_{excess} vs temperature for Ar melting at coverage $\rho=0.81$.

where d is the measured lattice constant of the incommensurate solid, and for a hexagonal lattice $q = 4\pi/\sqrt{3}d$.

In the melting studies of Xe, it was observed that the ratio of κ_{excess} to κ_{radial} was a constant approximately equal to 3 for the fluid phase.¹¹ We show in Fig. 12 a plot of this ratio for Ar. One can see that for our Ar data this ratio falls between 1 and 3 in the temperature range studied. However, the Ar data alone cannot support the conclusion that this ratio is a constant.

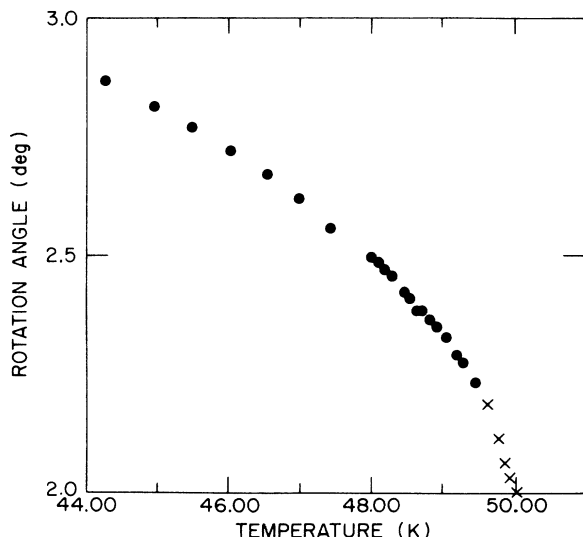


FIG. 10. Rotation angle vs temperature for Ar, at coverage $\rho=0.81$ with solid (●) and fluid (×) points shown.

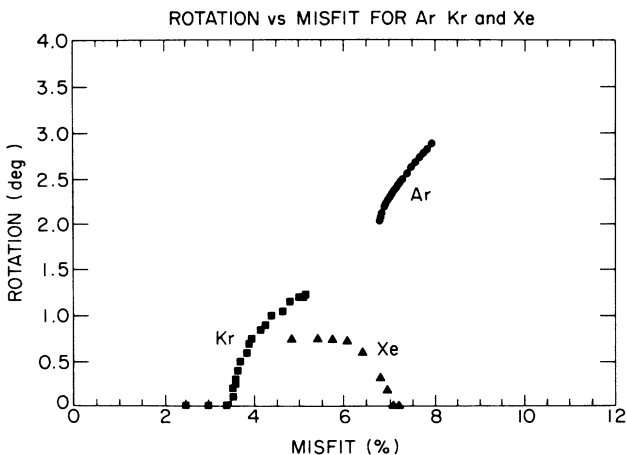


FIG. 11. Plot of rotation angle vs percent mean misfit m for Ar, Kr (Ref. 21), and Xe.

Xe ROTATION

Data were taken for the orientation angle of the incommensurate Xe solid as a function of temperature. The Xe was added to the cell to yield a coverage of $\rho=1.07$. Angle scans for the Xe solid are shown as a function of temperature in Fig. 13; the temperature and maximum in the corresponding radial scan are indicated. The Xe evolves from a rotated incommensurate solid phase to an aligned incommensurate solid phase. The data are shown as a function of misfit in Fig. 11, and summarized in Table II. The Xe solid with this coverage melts at ~ 135 K. Note that the Xe, unlike Kr and Ar, rotates to zero for increasing misfit; however, all three rotate to zero for increasing temperature.

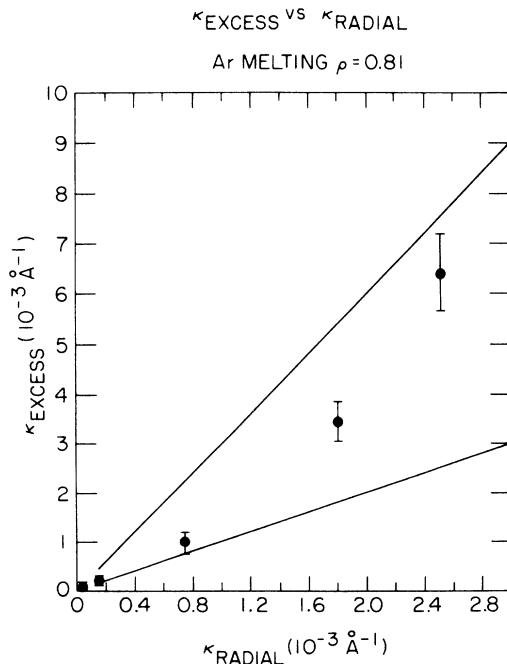


FIG. 12. Plot of κ_{excess} vs κ_{radial} . The solid lines represent a slope of 1 and 3.

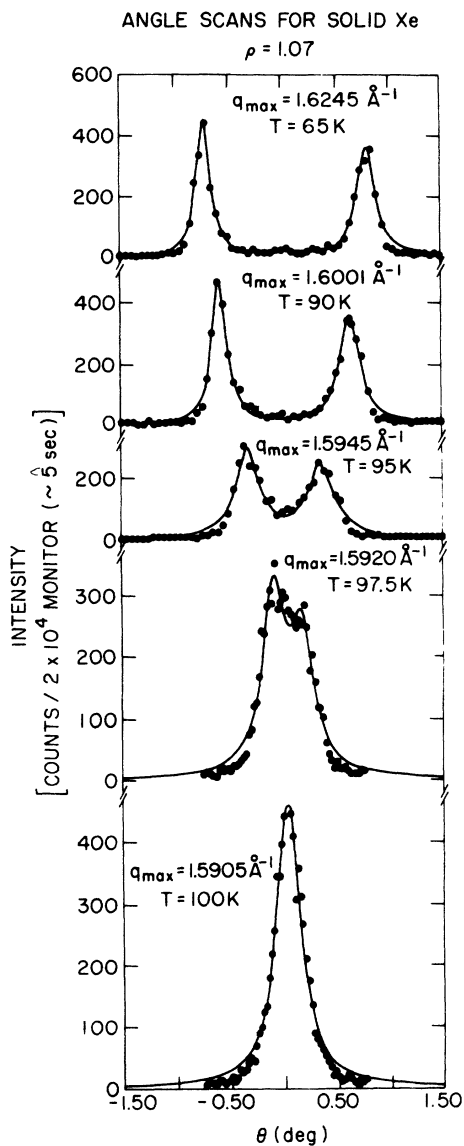


FIG. 13. Angular scans for Xe solid as a function of temperature as indicated; average $\rho \sim 1.07$.

DISCUSSION

The melting data for Ar and the rotational data for both Ar and Xe lead to an inescapable conclusion: The orienting field of the substrate plays a crucial role in the physics of these adsorbate/substrate systems.

The Ar melting transition at a coverage of $\rho = 0.81$ is clearly continuous (see Figs. 6 and 7); the monolayer system evolves continuously from the solid phase to a fluid phase with 400 Å correlation lengths. We saw no evidence for a discontinuous, abrupt change in either radial or angular width. Also, the 0.2% predicted change in lattice constant inferred from the Ar heat-capacity data¹² is 4 or more times larger than the smallest change in lattice constant observed between successive temperature steps (see Table I). Indeed the lattice constant undergoes a continuous 0.2% change from the solid value at T_m to

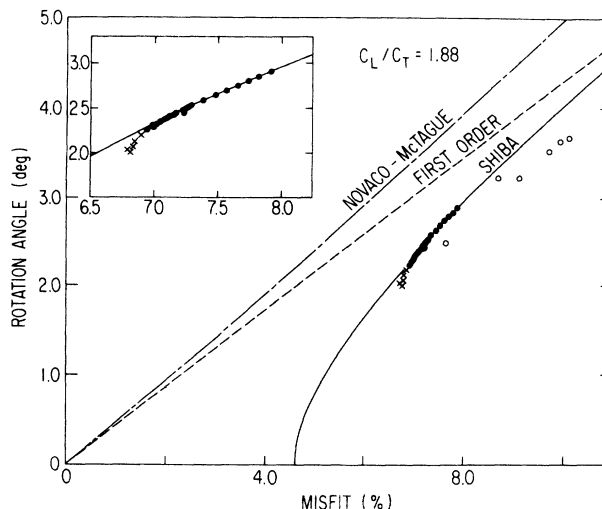


FIG. 14. Rotation angle versus percent misfit for Ar at coverage $\rho = 0.81$. The solid curve is the Shiba result for a critical misfit of 4.6% and a ratio $C_L/C_T = 1.88$. The Novaco-McTague (---) and first-order approximation (- · -) are shown. Inset: Expanded view of the Ar data. In both cases the fluid (x) and solid (●) points are indicated. The data from Shaw, *et al.* (Ref. 10) are shown as open circles.

the fluid value with $1/\kappa = 400$ Å.

Our data strongly support the data and conclusions of the Ar melting study performed on ZYX graphite.^{8,9} We have attempted to fit our κ versus T to the predicted functional form for the Kosterlitz-Thouless-Halperin-Nelson-Young (KTHNY) transition:

$$\kappa = \kappa_0 \exp\{-B/t^\nu\} \quad (3)$$

with $\kappa_0 = 0.06 \pm 0.02$, $B = 0.49 \pm 0.4$, and $T_m = 49.67 \pm 0.5$, where $t = (T - T_m)/T_m$ and ν is held at 0.369 as was done for the ZYX-graphite data. While only 4 data points determine the parameters in (3) our data follow the above curve with the same value of B as the ZYX-graphite data. We find a melting temperature of 49.67. Our data complement the ZYX-graphite data because we have studied a correlation length range for the fluid from ~ 1500 to 400 Å, while those data covered the range from 800 to 50 Å. The data can also satisfactorily be described by a power law $\kappa = \kappa_0 t^\nu$; the exponent was found to be $\nu = 0.43$. This exponent is not consistent with the $\nu = 0.83$ found in the ZYX-graphite study. Thus, the combined data of the ZYX-graphite study and the present single graphite crystal argue against the power law form and in favor of the universal form (3).

With regard to the excess angular width, the data are quite similar to Xe.¹⁸ Figure 12 illustrates that the ratio of κ_{excess} to κ_{rad} is in the range of 1–3 for Ar, whereas for Xe this ratio was ~ 2 –4. Thus, as with Xe, the positional correlations evolve with the excess angular width. It is the orientational epitaxy angle which distinguishes the Ar from the Xe.

Ar possesses a finite rotation angle at melting whereas Xe and Kr both melt from an aligned orientation. Since our data do not allow us to follow the rotation angle

TABLE I. Summary of Ar melting and rotation data.

Temperature (K)	Q_{\max} (\AA^{-1})	Misfit (%)	Rotation (deg)	Fitted $\kappa_{\text{radial}}^{-1}$ (10^{-4}\AA^{-1})	Fitted κ_{ang}^{-1} (10^{-4}\AA^{-1})
44.29(5)	1.8495(2)	7.92	2.872(2)	0.9(2)	1.7(4)
44.96(5)	1.8476(2)	7.83	2.816(2)	0.6(2)	1.6(4)
45.50(5)	1.8460(2)	7.75	2.776(2)	0.7(2)	2.0(4)
46.04(5)	1.8443(2)	7.66	2.724(2)	0.6(2)	1.9(4)
46.55(5)	1.8425(2)	7.57	2.673(2)	0.8(2)	1.5(4)
46.99(5)	1.8408(2)	7.49	2.619(2)	0.7(2)	1.6(4)
47.44(5)	1.8388(2)	7.39	2.557(2)	1.0(3)	1.5(6)
48.00(5)	1.8369(2)	7.29	2.496(2)	0.5(2)	1.9(4)
48.10(5)	1.8366(2)	7.27	2.485(2)	0.8(2)	1.8(4)
48.19(5)	1.8362(2)	2.47	2.474(2)	1.0(3)	1.7(6)
48.29(5)	1.8357(2)	7.23	2.460(2)	0.9(3)	1.6(6)
48.35(5)	1.8357(2)	7.23	2.460(2)	0.7(2)	1.9(4)
48.46(5)	1.8359(2)	7.24	2.425(2)	0.8(2)	1.8(4)
48.54(5)	1.8346(2)	7.17	2.412(2)	0.7(2)	1.9(4)
48.64(5)	1.8315(2)	7.02	2.404(2)	0.8(2)	1.8(4)
48.72(5)	1.8336(2)	7.12	2.387(2)	1.0(3)	2.3(6)
48.82(5)	1.8333(2)	7.11	2.368(2)	0.4(2)	1.8(4)
48.92(5)	1.8328(2)	7.08	2.351(2)	0.8(2)	1.8(4)
49.04(5)	1.8322(2)	7.05	2.327(2)	0.8(3)	2.6(6)
49.20(5)	1.8315(2)	7.02	2.291(2)	0.8(3)	2.5(6)
49.30(5)	1.8311(2)	7.00	2.274(2)	0.6(2)	2.2(4)
49.47(5)	1.8301(2)	6.94	2.233(2)	0.8(3)	2.5(6)
49.64(5)	1.8292(2)	6.90	2.187(2)	1.6(4)	3.6(8)
49.80(5)	1.8282(2)	6.85	2.116(2)	7.5(5)	17(1)
49.88(5)	1.828(1)	6.84	2.06(3)	18(3)	52(9)
49.96(5)	1.827(1)	6.79	2.03(3)	23(3)	53(7)
50.03(5)	1.827(1)	6.79	2.00(5)	25(5)	90(10)

below $\sim 2^\circ$, we can only speculate on the behavior of the rotation angle in the fluid which has a correlation length less than 400\AA . From the plot in Fig. 10, rotation angle is varying with temperature even at the melting temperature. If we extrapolate this curve linearly to a temperature above melting where the Ar from the ZYX data

possesses a 50\AA correlation length, we find that θ_{rot} would be $\sim 1.7^\circ - 1.8^\circ$.

But it is clear that rotation angle is not varying linearly with respect to temperature or with respect to misfit. The rotation angle rolls over more rapidly toward zero for decreasing misfit. This behavior has been addressed

TABLE II. Summary of Xe rotation data.

Temperature (K)	Q_{\max} (\AA^{-1})	Misfit (%)	Rotation degrees	Warming or cooling
95.0	1.5943(3)	-6.82	0.15	C
90.0	1.5999(3)	-6.44	0.31	C
85.0	1.6052(3)	-6.09	0.55	C
80.0	1.6102(3)	-5.76	0.64	C
75.0	1.6145(3)	-5.48	0.71	C
70.0	1.6182(3)	-5.24	0.75	C
65.0	1.6215(3)	-5.03	0.75	C
60.0	1.6240(3)	-4.86	0.75	C
55.0	1.6260(3)	-4.74	0.75	C
65.0	1.6245(3)	-4.83	0.72	W
75.0	1.6152(3)	-5.44	0.72	W
80.0	1.6107(3)	-5.73	0.73	W
85.0	1.6052(3)	-6.09	0.68	W
90.0	1.6001(3)	-6.43	0.60	W
95.0	1.5945(3)	-6.80	0.37	W
97.5	1.5920(3)	-6.97	0.10	W
100.0	1.5905(3)	-7.07	0.00	W
105.0	1.5896(3)	-7.13	0.00	W

by Shiba,^{23,24} and the explanation is tied into the effect of domain walls in the system. The description works quite well in the case of Kr on graphite, where the variation of rotation angle with misfit follows the Shiba prediction. We have made an effort to model this effect for Ar with the Shiba description. In the Shiba theory, the relationship between misfit and rotation angle is dependent upon two parameters: domain wall width, λ , and the ratio of the longitudinal and transverse speeds of sound for the overlayer, C_L/C_T . For Kr, the data were well described by fixing C_L/C_T to $\sqrt{3}$, corresponding to a Cauchy solid; the domain wall full width was then equal to ~ 6 Kr (10) row spacings. For Ar, the data can only be modeled if both λ and C_L/C_T are allowed to vary. The solid line through the data in Fig. 14 is the Shiba theory for a critical onset of 4.6% and a C_L/C_T ratio of 1.88. The line is obtained by the approximation of scaling the Shiba result for $C_L/C_T = \sqrt{3}$ from Ref. 24. This is not unphysical since substrate-induced stress has been predicted to renormalize C_L/C_T . Furthermore, a transverse softening must be expected at melting. For comparison with the Shiba treatment, we show two additional curves in Fig. 14. The dot-dashed curve is the Novaco-McTague result at zero misfit. The straight line is the first-order result. It agrees with the Novaco-McTague line for small misfit, while it agrees with the Shiba curve for large misfit.¹⁴

Clearly, the overall agreement with the Shiba theory is not good. The last four to six data points which are in the fluid phase deviate from this curve. The resulting curve predicts that the rotation angle will rotate to zero at a misfit of $\sim 4.6\%$ ($q = 1.7851 \text{ \AA}$, $D = 4.064 \text{ \AA}$). This corresponds to a 1.5% expansion of the lattice constant relative to the largest lattice constant observed for Ar fluid in the ZYX study. Another estimate for the critical misfit would be $\sim 6\%$ which is obtained by extrapolating the curve including the data points from the fluid. But, 6.8% is the smallest misfit for which we observe a diffraction peak.

We did not find any evidence for a peak at zero rotation angle, but we cannot rule out the possibility that such a peak was merely too weak for us to observe.

It is a prediction of the KTHNY theory that in the fluid phase the peak intensity A and the width κ scale as $\kappa^{-2+\eta}$ (Ref. 2). This was tested in both the Xe and Ar ZYX-graphite studies and an η of about 0.3 was inferred.^{9,16} We have attempted to test this scaling relation with the data in the present study and have found that the single-crystal data do not seem to obey this scaling relation, but there is too much scatter for a rigorous test.

Figure 11 shows the misfit versus rotation data for Xe. Since Xe is incommensurate in expansion relative to the commensurate $(\sqrt{3} \times \sqrt{3})R30^\circ$ structure, the misfit is negative. Thus, Xe appears to rotate to zero for increasing $|m|$, in contrast to both Ar and Kr. However all three do rotate to zero with increasing temperature. Both the Novaco-McTague and Shiba descriptions of orientational epitaxy are zero temperature theories which neglect the effects of entropy. While the Novaco-McTague theory is a linear-response calculation, the Shiba theory includes the topology of the hexagonal domain-wall lattice. Therefore, in the latter, the over-

layer is predicted to be rotationally aligned until a finite misfit, the critical misfit for rotation. The existence of large domains and long domain walls thus energetically favors the overlayer's alignment with the substrate. Numerous authors have pointed out that the hexagonal domain wall network provides a canonical way to introduce entropy to the structure.^{25,26,27} The domain wall network can fluctuate or "breathe" such that the total domain wall length and the number of domains is preserved. Only the energy associated with the domain wall interaction is altered in such a fluctuation. At high temperature one must then expect constant fluctuations in the domain sizes. The majority of atoms in the overlayer must therefore be in domains the sizes of which are larger than the nominal size given by the misfit. Thus, we suggest that the effect of temperature can be described by an interaction between the overlayer and the substrate which is dominated by domains larger than the average size; i.e., the epitaxial angle will tend to be small with increasing temperature. If the effective domain size becomes larger than the critical value for the onset of rotation then the effect of temperature is to realign the overlayer with the substrate. This is exactly the observed behavior for Xe. Further, because Xe has a relatively weaker interaction with the substrate than Ar the domain walls will be less pronounced. Consequently fluctuations in the domain wall network in a Xe monolayer should be more pronounced than in the Ar at the same reduced temperature. This may explain the qualitatively different behavior for the epitaxy in the two systems.

CONCLUSION

We have studied the melting behavior for Ar at a coverage of $\rho \sim 0.81$ and the orientational epitaxy effect for Ar and Xe. We find that the Ar melts continuously from a rotated incommensurate solid to a rotated fluid phase—the fluid with positional correlations is rotated by $\sim 2^\circ$. The melting behavior agrees well with that observed by x-ray diffraction using a ZYX-graphite substrate, and is consistent with the heat capacity data of Migone *et al.* insofar as the monolayer loses its correlations from 1500 to 400 \AA in a temperature interval of width 0.3 K. For Xe, the orientational epitaxy data show a rotation to zero for increasing $|m|$, contrary to the Ar and Kr behavior. This is discussed in light of the role of entropy in the structure of this system, and also the relatively lower susceptibility of the Xe overlayer to the substrate potential. These data underscore the important role of the substrate in determining the behavior of these overlayer systems.

ACKNOWLEDGMENTS

We wish to thank M. Nielsen, S. C. Fain, Jr., J. Z. Larese, L. Passell, and A. D. Novaco for many helpful discussions. One of us (K.L.D.) is grateful to the Department of Physics at Risø National Laboratory (Roskilde, Denmark) for hospitality extended while carrying out the

data analysis for this paper. Work done at the Stanford Synchrotron Radiation Laboratory (Palo Alto, CA) was supported by the U.S. Department of Energy (Office of Basic Energy Sciences). Work done at Brookhaven Na-

tional Laboratory was supported by the U.S. Department of Energy under Contract No. DE-AC02-76CH00016. We also acknowledge support from the Danish Natural Science Foundation.

-
- ¹J. M. Kosterlitz and D. J. Thouless, *J. Phys. C* **6**, 1181 (1973).
²B. I. Halperin and D. R. Nelson, *Phys. Rev. Lett.* **41**, 121 (1978); **41**, 519(E) (1978).
³D. R. Nelson and B. I. Halperin, *Phys. Rev. B* **19**, 2457 (1979).
⁴A. P. Young, *Phys. Rev. B* **19**, 1855 (1979).
⁵W. A. Steele, *Surf. Sci.* **36**, 317 (1973).
⁶G. Vidali and M. W. Cole, *Phys. Rev. B* **29**, 6736 (1984).
⁷H. Taub, L. Passell, J. K. Kjems, K. Carneiro, J. P. McTague, and J. G. Dash, *Phys. Rev. Lett.* **34**, 654 (1975); H. Taub, K. Carneiro, J. K. Kjems, L. Passell, and J. P. McTague, *Phys. Rev. B* **16**, 4551 (1977).
⁸J. P. McTague, J. Als-Nielsen, J. Bohr, and M. Nielsen, *Phys. Rev. B* **25**, 7765 (1982).
⁹M. Nielsen, J. Als-Nielsen, J. Bohr, J. P. McTague, D. E. Moncton, and P. W. Stephens, *Phys. Rev. B* **35**, 1419 (1987).
¹⁰C. G. Shaw, S. C. Fain, Jr., and M. D. Chinn, *Phys. Rev. Lett.* **41**, 955 (1978).
¹¹T. T. Chung, *Surf. Sci.* **87**, 438 (1979).
¹²A. D. Migone, Z. R. Li, and M. H. W. Chan, *Phys. Rev. Lett.* **53**, 810 (1984).
¹³A. D. Novaco and J. P. McTague, *Phys. Rev. Lett.* **38**, 1286 (1977).
¹⁴J. P. McTague and A. D. Novaco, *Phys. Rev. B* **19**, 5299 (1977).
¹⁵S. C. Fain (private communication).
¹⁶P. A. Heiney, P. W. Stephens, R. J. Birgeneau, P. M. Horn, and D. E. Moncton, *Phys. Rev. B* **28**, 6416 (1983); P. A. Heiney, Ph.D. thesis, Massachusetts Institute of Technology, 1982.
¹⁷P. Dimon, P. M. Horn, M. Sutton, R. J. Birgeneau, and D. E. Moncton, *Phys. Rev. B* **31**, 437 (1985).
¹⁸E. D. Specht, R. J. Birgeneau, K. L. D'Amico, D. E. Moncton, S. E. Nagler, and P. M. Horn, *J. Phys. (Paris) Lett.* **46**, L561 (1985).
¹⁹K. L. D'Amico and D. E. Moncton, *J. Vac. Sci. Tech.* **A4**, 1455 (1986).
²⁰D. E. Moncton and G. S. Brown, *Nucl. Instrum. Methods* **208**, 579 (1983).
²¹K. L. D'Amico, D. E. Moncton, E. D. Specht, R. J. Birgeneau, S. E. Nagler, and P. M. Horn, *Phys. Rev. Lett.* **53**, 2250 (1984).
²²J. Bohr, Ph.D. thesis, Technical University of Denmark, 1984.
²³H. Shiba, *J. Phys. Soc. Jpn.* **46**, 1852 (1979).
²⁴H. Shiba, *J. Phys. Soc. Jpn.* **48**, 211 (1980).
²⁵S. N. Coppersmith, D. S. Fisher, B. I. Halperin, P. A. Lee, and W. F. Brinkman, *Phys. Rev. Lett.* **46**, 549 (1981).
²⁶M. Kardar and A. N. Berker, *Phys. Rev. Lett.* **48**, 1552 (1982).
²⁷M. B. Gordon and J. Villain, *J. Phys. C* **15**, 1817 (1982).